Commun. Comput. Phys.
doi: 10.4208/cicp.220415.080816a

Vol. **21**, No. 3, pp. 782-807
March 2017

Solving Vlasov-Poisson-Fokker-Planck Equations using NRxx method

Yanli Wang[1,*] and Shudao Zhang[1]

[1] *Institute of Applied Physics and Computational Mathematics, Beijing 100094, P.R. China.*

Received 22 April 2015; Accepted (in revised version) 8 August 2016

Abstract. We present a numerical method to solve the Vlasov-Poisson-Fokker-Planck (VPFP) system using the NRxx method proposed in [4, 7, 9]. A globally hyperbolic moment system similar to that in [23] is derived. In this system, the Fokker-Planck (FP) operator term is reduced into the linear combination of the moment coefficients, which can be solved analytically under proper truncation. The non-splitting method, which can keep mass conservation and the balance law of the total momentum, is used to solve the whole system. A numerical problem for the VPFP system with an analytic solution is presented to indicate the spectral convergence with the moment number and the linear convergence with the grid size. Two more numerical experiments are tested to demonstrate the stability and accuracy of the NRxx method when applied to the VPFP system.

AMS subject classifications: 35Q83, 65L20, 78M05

Key words: Moment closure, Fokker-Planck operator, VPFP system, spectral convergence.

1 Introduction

The Vlasov-Poisson-Fokker-Planck (VPFP) system describes the dynamics of the charged particles which are subject to the electrostatic force coming from their Coulomb interaction. It is obtained by adding a diffusion term (FP operator term) onto the Vlasov-Poisson (VP) equations. Though the stochastic modification is simple, the FP operator term greatly changes the properties of the VP equations.

The existence and uniqueness of the weak and classical solutions to the VPFP and related systems have been well studied. In [26], the uniqueness and stability of the weak solution to the VFP equation were proved by R. Rautmann. H. Neunzert in [24] generalized the results concerned with the existence and uniqueness of the solutions from

*Corresponding author. *Email addresses:* wang_yanli@iapcm.ac.cn (Y. Wang), zhang_shudao@iapcm.ac.cn (S. Zhang)

 ©2017 Global-Science Press

https://doi.org/10.4208/cicp.220415.080816a Published online by Cambridge University Press

the ordinary Vlasov equation to the VFP system using a probabilistic method. The fully deterministic proof of the existence of the global solutions to the VFP system in one and two space dimensions were proposed in [14], which also proved that the solutions to the VPFP system converged to those to the VP equations, when the coefficients in the FP operator term went to zero. The global existence of the solution to the VPFP system with small initial data was raised in [30]. Later on, F. Bouchut in [2,3] proved the existence and uniqueness of the smooth solution to the VPFP system in three dimensions. For the property of VPFP system, some other models are derived based on it. The high-field model of the VPFP system was studied in [17]. Moreover, the parabolic limit model of the VPFP system was discussed in [25].

Due to the complex phenomena in the plasma, the numerical simulation plays an important role in the study of the VPFP and related equations. For the stochastic properties of the FP operator, the random particle method is one of the most effective methods. An analysis of the method was raised in [18] and a computational study of it was carried out in [1, 27]. The finite difference scheme was also proposed for the periodic 1D VPFP system in [13, 28]. The deterministic methods, which approximated the solution along the characteristic curves associated with the transport part of the VPFP system were also proposed, eg. [19,27,28]. Further more, S. Wollman in [31,32] combined the deterministic particle type computation with a process of periodically reconstructing the distribution function on a fixed grid. This method was extended to the two dimension case and the Vlasov-Maxwell-Fokker-Planck system as well. In recent years, some asymptotic preserving schemes were proposed to solve the VPFP system under different field regions. For example, in the high-field regime, the forcing term containing the electric potential is stiff, and an explicit method would require $\Delta t \sim \min(\Delta x, \epsilon\Delta v)$, where $1/\epsilon$ is the stiff coefficient of the forcing term. Moreover, the diffusive nature of the Fokker-Planck operator poses the constrain $\Delta t \sim \mathcal{O}(\epsilon\Delta v^2)$. When ϵ is small, the numerical computation becomes quite expensive. Shu in [12] performed some numerical simulations on the high-field model. And the numerical method proposed in [22] could capture the high-field limit of the VPFP system using large time steps and coarse meshes. Besides, the spectral method was also used to solve the Fokker-Planck-Landau system in [15]. Recently, an approach based on the moment method was proposed in [29], and therein the distribution function was expanded using the Hermite polynomials with a prescribed macroscopic velocity chosen as the expansion center and a prescribed temperature of the particles as the scaling factor.

In the past years, a regularized moment method (the NRxx method) was developed in [4, 7, 9] to numerically solve the Boltzmann equation. The NRxx method adopts the Hermite polynomial expansion to approximate the distribution functions, with the basis function shifted by the local macroscopic velocity and scaled by the square root of the local temperature. The new regularized model proposed in [4, 5] guaranteed the global hyperbolicity of the regularized moment system. Due to the local well-posedness provided by the global hyperbolicity, it was eventually accessible that approximating the distribution functions far away from the equilibrium distribution by the stable simula-

https://doi.org/10.4208/cicp.220415.080816a Published online by Cambridge University Press

tion using large number of moments. Numerical experiments using the NRxx method to solve the large moment system were tested in [7, 8, 10]. And it has also been applied to solve the VP equations [11] and the Wigner equations [21, 23], where the convergence of the NRxx method was certified.

Inspired by the efficiency of the NRxx method, we in this paper apply it to the VPFP system, which is similar to the Vlasov equation in the convection term, while the source term is more complicated. Under the framework of the NRxx method, the forcing term with electric potential and the source term can be changed into the linear combination of the moment coefficients, and then can be solved analytically. This will eliminate the constrain on Δt even when the forcing term and the source term are stiff. According to the numerical resolution study, it is exhibited that our method is numerically converged with the comparison to the reference solution. With the increasing of the grid number, the numerical solutions are converging to the reference solution linearly. The spectral convergence is also derived with the variation of the number of moments. Two other examples are tested. One is the high-field model of the VPFP system, in which a Riemann problem is solved. The other is the approach to the steady state of the VPFP system. The electric energy and the kinetic energy are tested with different parameters. It shows that the parameters greatly impact the converging velocity to the steady state.

The layout of this paper is as follows: first, we give a short description and some properties of the VPFP system. In Section 3, the dimensionless case of the VPFP system is presented and the moment system derived by NRxx method is proposed. The detailed method to solve the source term brought by the FP operator is also raised in this section. Moreover, the conservation properties of the scheme are also discussed in this part. In the forth section, the numerical convergence based on the grid size and the moment number is discussed. Then, two numerical simulations are given. Related comparison and analysis are put forward too. Some concluding remarks are given in the last section.

2 Vlasov-Poisson-Fokker-Planck equations

The VPFP system is widely used to describe the Brownian motion of the particles. Let $f(t,\boldsymbol{x},\boldsymbol{v})$ be the distribution function of the particles at time t, velocity $\boldsymbol{v}$ and position $\boldsymbol{x}$. The VPFP system can be written as

$$\partial_t f+\boldsymbol{v}\cdot\nabla_{\boldsymbol{x}} f-\frac{q}{m_e}\nabla_{\boldsymbol{x}}\phi\cdot\nabla_{\boldsymbol{v}} f=\frac{1}{\tau_e}\mathcal{L}_{\mathcal{FP}}, \tag{2.1}$$

$$-\Delta_{\boldsymbol{x}}\phi=\frac{q}{\epsilon_0}(\rho-h(\boldsymbol{x})), \tag{2.2}$$

where ϵ_0 is the vacuum permittivity, q and m_e are elementary charge and mass of the particles, and τ_e is the relaxation time due to the collision of the particles with the surrounding bath [22]. The function $h(\boldsymbol{x})$ is a given positive background charge and satisfies

https://doi.org/10.4208/cicp.220415.080816a Published online by Cambridge University Press

the global neutrality relation:

$$\int_{\mathbb{R}^3\times\mathbb{R}^3} f(\boldsymbol{x},\boldsymbol{v})\,\mathrm{d}\boldsymbol{x}\mathrm{d}\boldsymbol{v}=\int_{\mathbb{R}^3} h(\boldsymbol{x})\,\mathrm{d}\boldsymbol{x}. \tag{2.3}$$

$\rho(t,\boldsymbol{x})$ in Eq. (2.1) is the density of the particles given by

$$\rho(t,\boldsymbol{x})=\int_{\mathbb{R}^3} f(t,\boldsymbol{x},\boldsymbol{v})\,\mathrm{d}\boldsymbol{v}, \tag{2.4}$$

and $\mathcal{L}_{\mathcal{FP}}$ is the FP operator term, which reads

$$\mathcal{L}_{\mathcal{FP}}=\nabla_{\boldsymbol{v}}\cdot(\boldsymbol{v}f+\mu_e\nabla_{\boldsymbol{v}}f), \tag{2.5}$$

where $\sqrt{\mu_e}=\sqrt{(k_BT_{th})/m_e}$ is the thermal velocity, k_B is the Planck constant, and T_{th} is the temperature of the bath.

We introduce some more macroscopic variables of the VPFP system:

$$\rho\boldsymbol{u}=\int_{\mathbb{R}^3}\boldsymbol{v}f\,\mathrm{d}\boldsymbol{v},\quad 3\rho\theta(t,\boldsymbol{x})=\int_{\mathbb{R}^3}|\boldsymbol{v}-\boldsymbol{u}|^2 f(t,\boldsymbol{x},\boldsymbol{v})\,\mathrm{d}\boldsymbol{v}, \tag{2.6}$$

$$\boldsymbol{q}=\frac{1}{2}\int_{\mathbb{R}^3}|\boldsymbol{v}-\boldsymbol{u}|^2(v_i-u_i)(t,\boldsymbol{x},\boldsymbol{v})\,\mathrm{d}\boldsymbol{v},\quad P_{ij}=\int_{\mathbb{R}^3}(v_i-u_i)(v_j-u_j)f(t,\boldsymbol{x},\boldsymbol{v})\,\mathrm{d}\boldsymbol{v}, \tag{2.7}$$

here $\boldsymbol{u}$ and $\theta(t,\boldsymbol{x})$ are the macroscopic velocity and the temperature of the particles respectively. $\boldsymbol{q}$ is the heat flux and P_{ij} is the pressure tensor.

The mass conservation and the balance law of momentum and energy of the VPFP system are as follows: $i=1,2,3$

$$\frac{\mathrm{d}}{\mathrm{d}t}\int_{\mathbb{R}^3\times\mathbb{R}^3} f(t,\boldsymbol{x},\boldsymbol{v})\,\mathrm{d}\boldsymbol{x}\mathrm{d}\boldsymbol{v}=0,\quad t\in\mathbb{R}^+, \tag{2.8}$$

$$\frac{\mathrm{d}}{\mathrm{d}t}\int_{\mathbb{R}^3\times\mathbb{R}^3} v_i f(t,\boldsymbol{x},\boldsymbol{v})\,\mathrm{d}\boldsymbol{x}\mathrm{d}\boldsymbol{v}+\int_{\mathbb{R}^3}\left(\frac{q}{m_e}\frac{\partial\phi}{\partial x_i}\right)\rho\,\mathrm{d}\boldsymbol{x}=-\int_{\mathbb{R}^3}\rho u_i\,\mathrm{d}\boldsymbol{x}, \tag{2.9}$$

$$\frac{1}{2}\frac{\mathrm{d}}{\mathrm{d}t}\left(\int_{\mathbb{R}^3\times\mathbb{R}^3}|\boldsymbol{v}|^2 f(t,\boldsymbol{x},\boldsymbol{v})\,\mathrm{d}\boldsymbol{x}\mathrm{d}\boldsymbol{v}+\int_{\mathbb{R}^3}|E(t,\boldsymbol{x})|^2\mathrm{d}\boldsymbol{x}\right)$$
$$=\int_{\mathbb{R}^3}\left[-(\rho|\boldsymbol{u}|^2+3\rho\theta)+3\mu_e\rho\right]\mathrm{d}\boldsymbol{x}. \tag{2.10}$$

3 Numerical method

3.1 The moment system

For the similar form of the VPFP system and the Wigner equation, we extend the moment method derived in [6] to the VPFP system. In this section, we introduce briefly the

https://doi.org/10.4208/cicp.220415.080816a Published online by Cambridge University Press

derivation of the moment systems. Without loss of generality, we consider the 1D form of the VPFP system as below:

$$\frac{\partial f}{\partial t}+v\frac{\partial f}{\partial x}-\frac{\partial \phi}{\partial x}\frac{\partial f}{\partial v}=\beta\left(\frac{\partial (vf)}{\partial v}+\gamma\frac{\partial^2 f}{\partial v^2}\right), \tag{3.1}$$

$$-\frac{\partial^2 \phi}{\partial x^2}=\rho-h, \tag{3.2}$$

where β and γ are two positive parameters decided by the bath [37]. In this case, the pressure tensor and the heat flux change into

$$P=\int_{\mathbb{R}}(v-u)^2 f(t,x,v)\,\mathrm{d}v=\rho\theta,\quad q=\frac{1}{2}\int_{\mathbb{R}}(v-u)^3 f\,\mathrm{d}v. \tag{3.3}$$

The distribution function $f(t,x,v)$ is expanded to a series of Hermite functions

$$f(t,x,v)=\sum_{\alpha\in\mathbb{N}} f_\alpha(t,x)\mathcal{H}_{\theta,\alpha}\left(\frac{v-u(t,x)}{\sqrt{\theta(t,x)}}\right), \tag{3.4}$$

where $\theta(t,x)$ is the local temperature and $u(t,x)$ is the local macroscopic velocity of the particles. Here $\mathcal{H}_{\theta,\alpha}(s)$ is defined by a multiplication of $\exp(-s^2/2)$ and the Hermite polynomial of order α, i.e.

$$\begin{aligned}\mathcal{H}_{\theta,\alpha}(s)&=\frac{1}{\sqrt{2\pi}}\theta^{-\frac{\alpha+1}{2}}\exp(-s^2/2)He_\alpha(s)\\&=(-1)^n\frac{1}{\sqrt{2\pi}}\theta^{-\frac{\alpha+1}{2}}\frac{\mathrm{d}^n}{\mathrm{d}s^n}\exp(-s^2/2).\end{aligned} \tag{3.5}$$

For any particular number $u'(t,x)$ and $\theta'(t,x)$, if the distribution function is expanded as

$$f(t,x,v)=\sum_{\alpha\in\mathbb{N}} f'_\alpha(t,x)\mathcal{H}_{\theta',\alpha}\left(\frac{v-u'(t,x)}{\sqrt{\theta'(t,x)}}\right), \tag{3.6}$$

then the following relations hold

$$\rho=f'_0, \tag{3.7}$$

$$\rho u=\rho u'+f_1, \tag{3.8}$$

$$\rho|u|^2+\rho\theta=2\rho uu'-\rho|u'|^2+\theta' f'_0+2f'_2. \tag{3.9}$$

In the case of $u'=u$ and $\theta'=\theta$, the following relations between the coefficients f_α can be verified:

$$f_0=\rho(t,x),\quad f_1=0,\quad f_2=0. \tag{3.10}$$

https://doi.org/10.4208/cicp.220415.080816a Published online by Cambridge University Press

Using the recursion relation and differential relation of the Hermite polynomial

$$He_{n+1}(s)=sHe_n(s)-nHe_{n-1}(s); \tag{3.11}$$

$$He_n'(s)=nHe_{n-1}(s); \tag{3.12}$$

to simplify the FP operator term and let

$$\xi=\frac{v-u(t,x)}{\sqrt{\theta(t,x)}}. \tag{3.13}$$

From Eq. (3.4), we can derive that

$$\frac{\partial f}{\partial v}=\sum_{\alpha=0}^{\infty}f_\alpha\frac{\partial}{\partial v}\mathcal{H}_{\theta,\alpha}(\xi)=\sum_{\alpha=0}^{\infty}f_\alpha[-\mathcal{H}_{\theta,\alpha+1}(\xi)]=\sum_{\alpha=1}^{\infty}-f_{\alpha-1}\mathcal{H}_{\theta,\alpha}(\xi), \tag{3.14}$$

$$\frac{\partial^2 f}{\partial v^2}=\sum_{\alpha=0}^{\infty}f_\alpha\frac{\partial^2}{\partial v^2}\mathcal{H}_{\theta,\alpha}(\xi)=\sum_{\alpha=0}^{\infty}f_\alpha[\mathcal{H}_{\theta,\alpha+2}(\xi)]=\sum_{\alpha=2}^{\infty}f_{\alpha-2}\mathcal{H}_{\theta,\alpha}(\xi). \tag{3.15}$$

Thus the FP operator term can be simplified as

$$\begin{aligned}\beta\left(\frac{\partial(vf)}{\partial v}+\gamma\frac{\partial^2 f}{\partial v^2}\right)=&\beta\sum_{\alpha=0}^{\infty}f_\alpha\mathcal{H}_{\theta,\alpha}+\beta\sum_{\alpha=0}^{\infty}-(\alpha+1)f_\alpha\mathcal{H}_{\theta,\alpha}\\&+\beta\sum_{\alpha=2}^{\infty}(-f_{\alpha-2})\theta\mathcal{H}_{\theta,\alpha}+\beta\sum_{\alpha=1}^{\infty}-f_{\alpha-1}u\mathcal{H}_{\theta,\alpha}\\&+\beta\gamma\left[\sum_{\alpha=2}^{\infty}f_{\alpha-2}\mathcal{H}_{\theta,\alpha}\right],\end{aligned} \tag{3.16}$$

and the force term can be simplified as

$$-\frac{\partial\phi}{\partial x}\frac{\partial f}{\partial v}=\frac{\partial\phi}{\partial x}\sum_{\alpha=1}^{\infty}f_{\alpha-1}\mathcal{H}_{\theta,\alpha}(\xi). \tag{3.17}$$

Assuming that the FP operator term and the force term can be written in the form below:

$$\frac{\partial\phi}{\partial x}\frac{\partial f}{\partial v}+\beta\left(\frac{\partial(vf)}{\partial v}+\gamma\frac{\partial^2 f}{\partial v^2}\right)=\sum_{\alpha\in\mathbb{N}}\mathcal{A}_\alpha\mathcal{H}_{\theta,\alpha}(\xi), \tag{3.18}$$

from Eq. (3.16) and Eq. (3.17), we can deduce that

$$\begin{aligned}&\mathcal{A}_0=0,\\&\mathcal{A}_1=\left(-\frac{\partial\phi}{\partial x}-\beta u\right)f_0-\beta f_1,\\&\mathcal{A}_2=-\beta(\theta-\gamma)f_0-\left(\frac{\partial\phi}{\partial x}+\beta u\right)f_1-2\beta f_2,\\&\mathcal{A}_\alpha=-\beta(\theta-\gamma)f_{\alpha-2}-\left(\frac{\partial\phi}{\partial x}+\beta u\right)f_{\alpha-1}-\alpha\beta f_\alpha,\quad \alpha>2.\end{aligned} \tag{3.19}$$

https://doi.org/10.4208/cicp.220415.080816a Published online by Cambridge University Press

Taking the temporal and spatial derivatives directly on the basis functions $\mathcal{H}_{\theta,\alpha}$, with the expansion (3.4), the term

$$\frac{\partial f}{\partial t}+v\frac{\partial f}{\partial x} \tag{3.20}$$

is expanded as

$$\begin{aligned}\sum_{\alpha\in\mathbb{N}}\Bigg\{&\left(\frac{\partial f_\alpha}{\partial t}+\frac{\partial u}{\partial t}f_{\alpha-1}+\frac{1}{2}\frac{\partial\theta}{\partial t}f_{\alpha-2}\right)\\&+\Bigg[\left(\theta\frac{\partial f_{\alpha-1}}{\partial x}+u\frac{\partial f_\alpha}{\partial x}+(\alpha+1)\frac{\partial f_{\alpha+1}}{\partial x}\right)\\&\quad+\frac{\partial u}{\partial x}(\theta f_{\alpha-2}+uf_{\alpha-1}+(\alpha+1)f_\alpha)\\&\quad+\frac{1}{2}\frac{\partial\theta}{\partial x}(\theta f_{\alpha-3}+uf_{\alpha-2}+(\alpha+1)f_{\alpha-1})\Bigg]\Bigg\}\mathcal{H}_{\theta,\alpha}\left(\frac{v-u}{\sqrt{\theta}}\right).\end{aligned} \tag{3.21}$$

Substituting Eq. (3.19) and Eq. (3.21) back into Eq. (3.1), and collecting coefficients for the same basis function, we get the following general moment equations with a slight rearrangement:

$$\begin{aligned}&\frac{\partial f_\alpha}{\partial t}+\left(\frac{\partial u}{\partial t}+u\frac{\partial u}{\partial x}\right)f_{\alpha-1}+\frac{1}{2}\left(\frac{\partial\theta}{\partial t}+u\frac{\partial\theta}{\partial x}\right)f_{\alpha-2}\\&\quad+\left[\frac{\partial u}{\partial x}(\theta f_{\alpha-2}+(\alpha+1)f_\alpha)+\frac{1}{2}\frac{\partial\theta}{\partial x}(\theta f_{\alpha-3}+(\alpha+1)f_{\alpha-1})\right]\\&\quad+\left(\theta\frac{\partial f_{\alpha-1}}{\partial x}+u\frac{\partial f_\alpha}{\partial x}+(\alpha+1)\frac{\partial f_{\alpha+1}}{\partial x}\right)=\mathcal{A}_\alpha.\end{aligned} \tag{3.22}$$

Following the method in [36], we deduce the mass conservation in case of $\alpha=0$ as

$$\frac{\partial f_0}{\partial t}+\left(u\frac{\partial f_0}{\partial x}+f_0\frac{\partial u}{\partial x}\right)=0. \tag{3.23}$$

If we set $\alpha=1$, Eq. (3.22) reduces into

$$f_0\left(\frac{\partial u}{\partial t}+u\frac{\partial u}{\partial x}\right)+\frac{\partial P}{\partial x}=-\left(\frac{\partial\phi}{\partial x}+\beta u\right)f_0. \tag{3.24}$$

Let $\alpha=2$ in Eq. (3.22), then we get

$$\frac{1}{2}f_0\left(\frac{\partial\theta}{\partial t}+u\frac{\partial\theta}{\partial x}\right)+3\frac{\partial f_3}{\partial x}+P\frac{\partial u}{\partial x}=-\beta P+\beta\gamma f_0. \tag{3.25}$$

Together with Eq. (3.23), we can derive

$$\frac{1}{2}\frac{\partial P}{\partial t}+\frac{1}{2}u\frac{\partial P}{\partial x}+\frac{3}{2}P\frac{\partial u}{\partial x}+3\frac{\partial f_3}{\partial x}=-\beta P+\beta\gamma f_0. \tag{3.26}$$

https://doi.org/10.4208/cicp.220415.080816a Published online by Cambridge University Press

Substituting Eq. (3.24) and Eq. (3.25) into Eq. (3.22), we eliminate the temporal derivatives of u and θ. Then the quasi-linear form of the moment system reads:

$$\begin{aligned}&\frac{\partial f_\alpha}{\partial t}-\frac{1}{f_0}\frac{\partial P}{\partial x}f_{\alpha-1}-\frac{1}{f_0}\left(\frac{\partial f_3}{\partial x}+f_3\frac{\partial u}{\partial x}\right)f_{\alpha-2}\\&\quad+\left[\frac{\partial u}{\partial x}(\theta f_{\alpha-2}+(\alpha+1)f_\alpha)+\frac{1}{2}\frac{\partial\theta}{\partial x}(\theta f_{\alpha-3}+(\alpha+1)f_{\alpha-1})\right]\\&\quad+\left(\theta\frac{\partial f_{\alpha-1}}{\partial x}+u\frac{\partial f_\alpha}{\partial x}\right)+(\alpha+1)\frac{\partial f_{\alpha+1}}{\partial x}=\mathcal{A}_\alpha,\quad\forall\alpha>2.\end{aligned}\tag{3.27}$$

We collect Eq. (3.23), Eq. (3.24), Eq. (3.26) and Eq. (3.27) together to obtain a moment system with infinite number of equations.

Truncating the expansion of the distribution function $f(t,x,v)$ at order M, and then adopting the regularization obtained in [4], we finally get the moment system as follows:

$$\frac{\partial \boldsymbol{w}}{\partial t}+\hat{\mathbf{M}}(\boldsymbol{w})\frac{\partial \boldsymbol{w}}{\partial x}=\mathbf{G}\boldsymbol{w},\tag{3.28}$$

where $\boldsymbol{w}=(\rho,u,P/2,f_3,\cdots,f_M)^T$ and $\hat{\mathbf{M}}$ is an $(M+1)\times(M+1)$ matrix which is defined as

$$\hat{\mathbf{M}}(\boldsymbol{w})\frac{\partial \boldsymbol{w}}{\partial x}=\mathbf{M}(\boldsymbol{w})\frac{\partial \boldsymbol{w}}{\partial x}-\mathcal{R}_{\mathcal{M}}I_M,\tag{3.29}$$

where M is also an $(M+1)\times(M+1)$ matrix, whose entries are given as the coefficients of the terms in Eq. (3.23), Eq. (3.24), Eq. (3.26) and Eq. (3.27) with derivatives of $\boldsymbol{w}$, and $\mathcal{R}_{\mathcal{M}}I_M$ is the regularization term [6], with I_M as the last column of the $(M+1)\times(M+1)$ identity matrix and $\mathcal{R}_{\mathcal{M}}$ defined as

$$\mathcal{R}_{\mathcal{M}}=(M+1)\left[f_M\frac{\partial u}{\partial x}+\frac{1}{2}f_{M-1}\frac{\partial\theta(t,x)}{\partial x}\right].\tag{3.30}$$

Moreover, the entries of G arise from the external forcing term and the FP operator; its explicit formula is

$G_{i,j}$	$j=i-2$	$j=i-1$	$j=i$	otherwise
$i=2$	$\times$	$-\left(\frac{\partial\phi}{\partial x}+\beta u\right)/\rho$	0	0
$i=3$	$\beta\gamma$	0	-2β	0
$i=4$	0	0	-3β	0
$i=5$	0	$-\left(\frac{\partial\phi}{\partial x}+\beta u\right)$	-4β	0
otherwise	$-\beta(P/u-\gamma)$	$-\left(\frac{\partial\phi}{\partial x}+\beta u\right)$	$-(i-1)\beta$	0

https://doi.org/10.4208/cicp.220415.080816a Published online by Cambridge University Press

We list the detailed moment system of Eq. (3.28) when $M=5$ as an example:

$$\begin{aligned}
&\frac{\partial\rho}{\partial t}+u\frac{\partial\rho}{\partial x}+\rho\frac{\partial u}{\partial x}=0,\\
&\frac{\partial u}{\partial t}+u\frac{\partial u}{\partial x}+\frac{1}{\rho}\frac{\partial P}{\partial x}=-\frac{\partial\phi}{\partial x}-\beta u,\\
&\frac{\partial P/2}{\partial t}+u\frac{\partial P/2}{\partial x}+\frac{3}{2}P\frac{\partial u}{\partial x}+3\frac{\partial f_3}{\partial x}=-2\beta P/2+\beta\gamma\rho,\\
&\frac{\partial f_3}{\partial t}-\frac{P^2}{2\rho^2}\frac{\partial\rho}{\partial x}+4f_3\frac{\partial u}{\partial x}+\frac{P}{2\rho}\frac{\partial P}{\partial x}+u\frac{\partial f_3}{\partial x}+4\frac{\partial f_4}{\partial x}=-3\beta f_3,\\
&\frac{\partial f_4}{\partial t}-\frac{5}{2}\frac{P}{\rho^2}f_3\frac{\partial\rho}{\partial x}+5f_4\frac{\partial u}{\partial x}-\frac{f_3}{\rho}\frac{\partial P}{\partial x}+\frac{P}{\rho}\frac{\partial f_3}{\partial x}+u\frac{\partial f_4}{\partial x}+5\frac{\partial f_5}{\partial x}=-\left(\frac{\partial\phi}{\partial x}+\beta u\right)f_3-4\beta f_4,\\
&\frac{\partial f_5}{\partial t}-\frac{f_4}{\rho}\frac{\partial P}{\partial x}-\frac{3f_3}{\rho}\frac{\partial f_3}{\partial x}+\frac{P}{\rho}\frac{\partial f_4}{\partial x}+u\frac{\partial f_5}{\partial x}=-\beta(P/u-\gamma)f_3-\left(\frac{\partial\phi}{\partial x}+\beta u\right)f_4-5\beta f_5.
\end{aligned}$$

3.2 The numerical method

The non-splitting method is used here to numerically solve the whole system. The numerical scheme adopted in the x-direction is the standard finite volume discretization. Suppose Γ_h to be a uniform mesh in $\mathbb{R}$, and each cell is identified by an index j. For a fixed $x_0\in\mathbb{R}$ and $\Delta x>0$,

$$\Gamma_h=\{T_j=x_0+(j\Delta x,(j+1)\Delta x):j\in\mathbb{Z}\}. \tag{3.31}$$

The approximation of the coefficients of the Hermite expansion of the distribution function f at $t=t_n$ is denoted as

$$f_\alpha^n(x)\approx f_{\alpha,j}^n,\quad x\in T_j, \tag{3.32}$$

where $f_{\alpha,j}^n$ is the approximation over the cell T_j at the n-th time step and then the discrete distribution function has the following Hermite expansion form

$$f_h^n(x,v)\approx f_j^n(v)=\sum_{\alpha\leqslant M}f_{\alpha,j}^n\mathcal{H}_{\theta_j^n,\alpha}\left(\frac{v-u_j^n}{\sqrt{\theta_j^n}}\right). \tag{3.33}$$

From the derivation in [6], the term $\mathbf{M}(\boldsymbol{w})$ results in the conservation part in the Grad-type moment system, while the term $\mathcal{R}_{\mathcal{M}}I_M$ only revises f_M. Therefore, the flux has two parts here: the first part is the convection part and the second part is the regularization part:

$$Q_j^n=K_{1,j}^n(v)+K_{2,j}^n(v), \tag{3.34}$$

where $K_{1,j}^n$ is the contribution of the term $\mathbf{M}(\boldsymbol{w})$ in Eq. (3.29) and $K_{2,j}^n$ is the contribution of the term $\mathcal{R}_{\mathcal{M}}I_M$ in Eq. (3.30). Here $K_{1,j}^n$ is discretized in the conservative formation as

$$K_{1,j}^n(v)=-\frac{1}{\Delta x}\left[F_{j+\frac{1}{2}}^n(v)-F_{j-\frac{1}{2}}^n(v)\right], \tag{3.35}$$

https://doi.org/10.4208/cicp.220415.080816a Published online by Cambridge University Press

where $F^n_{j+\frac{1}{2}}$ is the numerical flux between cell T_j and T_{j+1} at t^n. We use the HLL scheme in our numerical experiments following [9], which reads:

$$F^n_{j+\frac{1}{2}}(v)=\begin{cases} vf^n_j(v), & 0\leqslant\lambda^L_{j+\frac{1}{2}},\\ \dfrac{\lambda^R_{j+\frac{1}{2}}vf^n_j(v)-\lambda^L_{j+\frac{1}{2}}vf^n_{j+1}(v)+\lambda^L_{j+\frac{1}{2}}\lambda^R_{j+\frac{1}{2}}[f^n_{j+1}(v)-f^n_j(v)]}{\lambda^R_{j+\frac{1}{2}}-\lambda^L_{j+\frac{1}{2}}}, & \lambda^L_{j+\frac{1}{2}}<0<\lambda^R_{j+\frac{1}{2}},\\ vf^n_{j+1}(v), & 0\geqslant\lambda^R_{j+\frac{1}{2}}. \end{cases} \tag{3.36}$$

As for the regularization part, the DLM theory [34,35] is employed to define its weak solution. Since the regularization term $\mathcal{R}_{\mathcal{M}}I_M$ only revises the coefficient f_M, we have to calculate $K^n_{2,j}$ only when $\alpha=M$. Following the method in [8], $K^n_{2,j}$ is chosen as the form below

$$K^n_{2,j}=-\frac{1}{\Delta x}(\hat{W}^{n-}_{j+1/2}-\hat{W}^{n+}_{j-1/2})\mathcal{H}_{\theta^n_j,M}\left(\frac{v-u^n_j}{\sqrt{\theta^n_j}}\right), \tag{3.37}$$

where $\hat{W}^{n\pm}_{j+1/2}$ is defined by

$$\hat{W}^{n-}_{j+1/2}=\begin{cases} 0, & 0\leqslant\lambda^L_{j+1/2},\\ -\frac{\lambda^L_{j+1/2}}{\lambda^R_{j+1/2}-\lambda^L_{j+1/2}}g^n_{j+1/2}, & \lambda^L_{j+1/2}<0<\lambda^R_{j+1/2},\\ g^n_{j+1/2}, & 0\geqslant\lambda^R_{j+1/2}, \end{cases} \tag{3.38}$$

and

$$\hat{W}^{n+}_{j+1/2}=\begin{cases} -g^n_{j+1/2}, & 0\leqslant\lambda^L_{j+1/2},\\ -\frac{\lambda^R_{j+1/2}}{\lambda^R_{j+1/2}-\lambda^L_{j+1/2}}g^n_{j+1/2}, & \lambda^L_{j+1/2}<0<\lambda^R_{j+1/2},\\ 0 & 0\geqslant\lambda^R_{j+1/2}, \end{cases} \tag{3.39}$$

where

$$g^n_{j+1/2}=\frac{1}{2}(M+1)\left[\begin{pmatrix} f^n_{M,j+1}\\ \frac{1}{2}f^n_{M-1,j+1}\end{pmatrix}+\begin{pmatrix} f^n_{M,j}\\ \frac{1}{2}f^n_{M-1,j}\end{pmatrix}\right]^T\begin{pmatrix} u^n_{j+1}-u^n_j\\ \theta^n_{j+1}-\theta^n_j\end{pmatrix}. \tag{3.40}$$

The $\lambda^L_{j+\frac{1}{2}}$ and $\lambda^R_{j+\frac{1}{2}}$ above are the fastest signal speeds of $\hat{M}$ (see [4]) as

$$\begin{aligned}\lambda^L_{j+\frac{1}{2}}&=\min\{u^n_j-C_{M+1}\sqrt{\theta^n_j},u^n_{j+1}-C_{M+1}\sqrt{\theta^n_{j+1}}\},\\ \lambda^R_{j+\frac{1}{2}}&=\max\{u^n_j+C_{M+1}\sqrt{\theta^n_j},u^n_{j+1}+C_{M+1}\sqrt{\theta^n_{j+1}}\},\end{aligned} \tag{3.41}$$

where C_{M+1} is the greatest zero of $He_{M+1}(x)$, u is the macroscopic velocity of the particles, and θ is the local temperature. The formula of the signal speed is also used to

https://doi.org/10.4208/cicp.220415.080816a Published online by Cambridge University Press

determine the time step Δt^n by the CFL condition

$$\frac{\Delta t}{\Delta x}\max_j\{|\lambda^R_{j+1/2}|,|\lambda^L_{j+1/2}|\}<CFL. \tag{3.42}$$

Then, we derive the whole scheme of the VPFP system. Substituting Eq. (3.33) into Eq. (3.34), then the numerical flux of cell j at time $t=t^n$ can be written as

$$Q^n_j=\sum_{\alpha=0}^{M}Q^n_{j,\alpha}\left(\frac{v-u^n_j}{\sqrt{\theta^n_j}}\right). \tag{3.43}$$

If we expand the distribution function f_j as

$$f_j(v)=\sum_{\alpha\leqslant M}f_{\alpha,j}\mathcal{H}_{\theta^n_j,\alpha}\left(\frac{v-u^n_j}{\sqrt{\theta^n_j}}\right), \tag{3.44}$$

the FP operator term and the force term at cell j are expanded as

$$\left(\frac{\partial\phi}{\partial x}\right)^n_j\frac{\partial f}{\partial v}+\beta\left(\frac{\partial vf}{\partial v}+\gamma\frac{\partial^2 f}{\partial v^2}\right)=\sum_{\alpha\leqslant M}\mathcal{A}^n_{\alpha,j}\mathcal{H}_{\theta^n_j,\alpha}\left(\frac{v-u^n_j}{\sqrt{\theta^n_j}}\right), \tag{3.45}$$

where $\mathcal{A}^n_{\alpha,j}$ has the same form as that in Eq. (3.18) with $u=u^n_j$ and $\theta=\theta^n_j$. At time $t=t^n$, we discrete Eq. (3.28) as

$$\frac{\partial f_j}{\partial t}+Q^n_j=\left(\frac{\partial\phi}{\partial x}\right)^n_j\frac{\partial f_j}{\partial v}+\beta\left(\frac{\partial vf_j}{\partial v}+\gamma\frac{\partial^2 f_j}{\partial v^2}\right). \tag{3.46}$$

Remark 3.1. Since u^n_j and θ^n_j are the local velocity and temperature of f^n_j instead of f_j here, $f_{1,j}$ and $f_{2,j}$ in Eq. (3.44) are not necessarily zero.

Collecting the coefficients of the same basis function, we get

$$\frac{\mathrm{d}\hat{\boldsymbol{w}}_j}{\mathrm{d}t}+\hat{Q}^n_j=\hat{\mathbf{G}}^n_j\hat{\boldsymbol{w}}_j, \tag{3.47}$$

where $\hat{\boldsymbol{w}}_j=(f_{0,j},f_{1,j},f_{2,j},\cdots,f_{M,j})$, and the entries of $\hat{\mathbf{G}}^n_j$ is

$G_{i,j}$	$j=i-2$	$j=i-1$	$j=i$	otherwise
$i=2$	$\times$	$-\left(\frac{\partial\phi^n_j}{\partial x}+\beta u^n_j\right)$	$-\beta$	0
$i=3$	$-\beta(\theta^n_j-\gamma)$	$-\left(\frac{\partial\phi^n_j}{\partial x}+\beta u^n_j\right)$	-2β	0
otherwise	$-\beta(\theta^n_j-\gamma)$	$-\left(\frac{\partial\phi^n_j}{\partial x}+\beta u^n_j\right)$	$-(i-1)\beta$	0

https://doi.org/10.4208/cicp.220415.080816a Published online by Cambridge University Press

The detailed form of (3.47) is

$$\begin{aligned}
&\frac{\mathrm{d}f_{0,j}}{\mathrm{d}t}+Q^n_{j,0}=0,\\
&\frac{\mathrm{d}f_{1,j}}{\mathrm{d}t}+Q^n_{j,1}=\left(-\frac{\partial\phi^n_j}{\partial x}-\beta u^n_j\right)f_{0,j}-\beta f_{1,j},\\
&\frac{\mathrm{d}f_{2,j}}{\mathrm{d}t}+Q^n_{j,2}=-\beta(\theta^n_j-\gamma)f_{0,j}-\left(\frac{\partial\phi^n_j}{\partial x}+\beta u^n_j\right)f_{1,j}-2\beta f_{2,j},\\
&\frac{\mathrm{d}f_{\alpha,j}}{\mathrm{d}t}+Q^n_{j,\alpha}=-\beta(\theta^n_j-\gamma)f_{\alpha-2,j}-\left(\frac{\partial\phi^n_j}{\partial x}+\beta u^n_j\right)f_{\alpha-1,j}-\alpha\beta f_{\alpha,j},\quad \alpha>2.
\end{aligned}\tag{3.48}$$

Remark 3.2. In Eq. (3.48), the matrix $\hat{\mathbf{G}}^n_j$ is constant, and it can be analytically solved recursively. We can just analytically solve Eq. (3.48) from $t=0$ to $t=\Delta t^n$, using f^n_j as the initial data. Δt^n is only decided by Eq. (3.42) and there is no restriction of the time step length, for the stiff term can be solved analytically.

Remark 3.3. After analytically solving Eq. (3.48), we can get the expansion of distribution function f^{n+1}_j at the expansion center u^n_j and the scaling factor θ^n_j. We have to rewrite f^{n+1}_j as

$$f^{n+1}_j(v)=\sum_{\alpha\leqslant M}f^{n+1}_{\alpha,j}\mathcal{H}_{\theta^{n+1}_j,\alpha}\left(\frac{v-u^{n+1}_j}{\sqrt{\theta^{n+1}_j}}\right),\tag{3.49}$$

where u^{n+1}_j and θ^{n+1}_j are the local macroscopic velocity and temperature of f^{n+1}_j decided by Eq. (2.6). And $f^{n+1}_{1,j}=f^{n+1}_{2,j}=0$ in Eq. (3.49). The techniques on the rewriting method have been clarified in detail in [9].

3.3 Outline of the algorithm

Suppose the coefficients $\boldsymbol{w}^n_j, j=1,\cdots,N$ of f^n_j have been obtained, we summarize the overall numerical scheme for one time step as follows:

1. *Calculate Δt^n according to the CFL condition Eq.* (3.42)*;*
2. *Obtain the numerical flux Q^n_j according to Eq.* (3.34)*;*
3. *Obtain ϕ^n_j using ρ^n_j;*
4. *Obtain the matrix $\hat{\mathbf{G}}^n_j$ using u^n_j, θ^n_j;*
5. *Obtain $\hat{\boldsymbol{w}}^{n+1,*}_j$ by solving Eq.* (3.48)*;*
6. *Update the velocity and temperature in each cell, and then obtain $\boldsymbol{w}^{n+1}_j$.*

https://doi.org/10.4208/cicp.220415.080816a Published online by Cambridge University Press

Remark 3.4. Since the accuracy of the numerical flux is first order, the accuracy of the whole numerical algorithm is only first order, even if Eq. (3.48) is solved analytically. Moreover, due to the complex form of the equation system, solving analytically is quite expensive. Therefore, high order Runge-Kutta scheme is always adopted to enlarge the time step and reduce the numerical complexity as well. The specific scheme of solving Eq. (3.48) using the first order explicit Euler method is:

$$f_j^{n+1}=f_j^n+\frac{\Delta t^{n,*}}{\Delta x}\sum_{\alpha=0}^{N}(\mathcal{A}_{\alpha,j}^n-Q_{\alpha,j}^n)\mathcal{H}_{\theta_j^n,\alpha}\left(\frac{v-u_j^n}{\sqrt{\theta_j^n}}\right). \tag{3.50}$$

And the time step $\Delta t^{n,*}$ in this case is

$$\frac{\Delta t^{n,*}}{\Delta x}\max_j\{|\lambda_{j+1/2}^R|,|\lambda_{j+1/2}^L|,|\lambda_{\hat{G}_j^n}|\}<CFL, \tag{3.51}$$

where $|\lambda_{\hat{G}_j^n}|$ is the maximum absolute value of the eigenvalue of matrix $\hat{\mathbf{G}}_j^n$. Since the matrix $\hat{\mathbf{G}}_j^n$ is constant in Eq. (3.48), its eigenvalue can be precomputed.

3.4 The conservative properties of the scheme

In this subsection, we will study the properties of the scheme. Let us denote the discretized mass as

$$\mathcal{D}_h(t_n)=\sum_{j=1}^{N}\Delta x\int_{v\in\mathbb{R}}f_j^n(v)\mathrm{d}v, \tag{3.52}$$

the discretized momentum of the particles as

$$\mathcal{M}_h(t_n)=\sum_{j=1}^{N}\Delta x\int_{v\in\mathbb{R}}vf_j^n\mathrm{d}v, \tag{3.53}$$

the total impulse due to the potential at the n-th time step as

$$\mathcal{P}_h(t_n)=\sum_{j=1}^{N}\Delta x\Delta t^n\left(\frac{\partial\phi}{\partial x}\right)_j^n\rho_j^n, \tag{3.54}$$

and the total impulse due to the FP operator term as

$$\mathcal{F}_h(t_n)=\sum_{j=1}^{N}\Delta x\Delta t^n u_j^n\rho_j^n. \tag{3.55}$$

Direct calculation gives us the following conclusion.

Theorem 3.1. *The numerical solution $f_h^n(x,v)$ given by the scheme satisfies that:*

https://doi.org/10.4208/cicp.220415.080816a Published online by Cambridge University Press

1. *Conservation of total mass:* $\mathcal{D}_h(t_n)=\mathcal{D}_h(t_0)$;

2. *Balance law of total momentum:* $\mathcal{M}_h(t_n)=\mathcal{M}_h(t_0)+\sum_{k=0}^{n-1}\mathcal{P}_h(t_k)+\sum_{k=0}^{n-1}\mathcal{F}_h(t_k)$,

in the case of the periodic boundary condition.

Proof. We check these two items one by one.

1. Conservation of mass:

   Noticing that the mass on each cell is not modified when we apply the regularization term and the FP source term, the conservation of the mass is straight forward based on results in [9].

2. Balance law of momentum:

   For the balance law of momentum, we need only verify

$$\mathcal{M}_h(t_{n+1})=\mathcal{M}_h(t_n)+\mathcal{P}_h(t_n)+\mathcal{F}_h(t_n). \tag{3.56}$$

   Here, we take the first order explicit Euler method as an example. From Eq. (3.50), let $\xi_j^n=(v-u_j^n)/\sqrt{\theta_j^n}$, we can derive

$$\begin{aligned}
&\mathcal{M}_h(t_{n+1})\\
&=\sum_{j=1}^{N}\Delta x\int_{v\in\mathbb{R}} v\left(f_j^n+\frac{\Delta t^n}{\Delta x}\sum_{\alpha=0}^{N}(\mathcal{A}_{\alpha,j}^n-Q_{\alpha,j}^n)\mathcal{H}_{\theta_j^n,\alpha}\left(\xi_j^n\right)\right)\mathrm{d}v\\
&=\sum_{j=1}^{N}\Delta x\int_{v\in\mathbb{R}} vf_j^n\mathrm{d}v+\int_{v\in\mathbb{R}}\sum_{j=1}^{N}v\Delta t^n\sum_{\alpha=0}^{M}\mathcal{A}_{\alpha,j}^n\mathcal{H}_{\theta_j^n,\alpha}\left(\xi_j^n\right)\mathrm{d}v\\
&\quad-\int_{v\in\mathbb{R}}\sum_{j=1}^{N}v\Delta t\sum_{\alpha=0}^{M}Q_{\alpha,j}^n\mathcal{H}_{\theta_j^n,\alpha}\left(\xi_j^n\right)\mathrm{d}v\\
&=\mathcal{M}_h(t_n)+\mathcal{F}_{h,1}+\mathcal{F}_{h,2}.
\end{aligned}$$

   Then we have to verify that $\mathcal{F}_{h,1}+\mathcal{F}_{h,2}$ equals to the total impulse. From the specific form of the numerical flux $Q_{\alpha,j}^n$ and the similar proof in [23], we have

$$\mathcal{F}_{h,2}=0. \tag{3.57}$$

   As to $\mathcal{F}_{h,1}$, thanks to Eq. (3.50), Eq. (3.19) and the orthogonality of the Hermite polynomial, we can derive that

$$\mathcal{F}_{h,1}=\sum_{j=1}^{N}\Delta t^n\int_{v\in\mathbb{R}} v\mathcal{A}_{1,j}^n\mathcal{H}_{\theta,1}\left(\xi_j^n\right)\mathrm{d}v=-\sum_{j=1}^{N}\Delta x\Delta t^n\left(-\left(\frac{\partial\phi}{\partial x}\right)_j^n-u_j^n\right)\rho_j^n. \tag{3.58}$$

https://doi.org/10.4208/cicp.220415.080816a Published online by Cambridge University Press

With Eq. (3.57) and Eq. (3.58), we can conclude the balance law of the total momentum consequently

$$\mathcal{M}_h(t_{n+1}) = \mathcal{M}_h(t_n) + \mathcal{P}_h(t_n) + \mathcal{F}_h(t_n). \tag{3.59}$$

The proof is completed. □

Remark 3.5. The above property of the scheme is kept to any time discretization method, and the explicit Euler method is only taken as an example in the proof.

4 Numerical results

In this section, the computational result of the VPFP system is presented to demonstrate the effectiveness of the NRxx method.

The computational examples are from [16, 22, 31]. The POSIX multi-threaded technique is used in our simulation, and at most 22 CPU cores are used.

4.1 Numerical resolution study

First, we examine the numerical convergence on different spatial grid size of the NRxx method. We will apply the numerical method to the simplified VPFP system as below:

$$\frac{\partial f}{\partial t} = -v\frac{\partial f}{\partial x} + \frac{\partial (vf)}{\partial v} + \frac{\partial^2 f}{\partial v^2}, \quad |x| \le 1, \ \ |v| < \infty. \tag{4.1}$$

The main reason for choosing the above test example is that its analytic solution can be found and this enables us to test the numerical convergence of the scheme applied to the simplified VPFP system. One of the exact solutions of Eq. (4.1) is

$$f(t,x,v) = \frac{1}{2}\left(2+\cos\left(\frac{\pi}{2}[x-(1-e^{-t})v]q(t)\right)\right)\exp\left(\frac{-v^2}{2}\right), \tag{4.2}$$

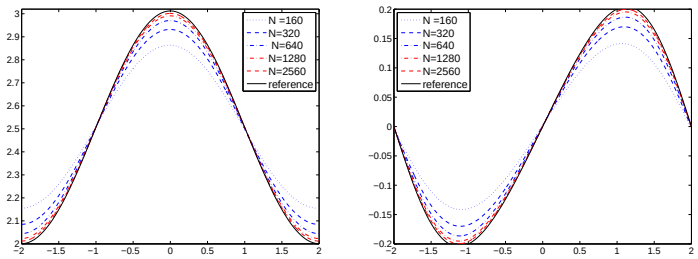
where

$$q(t) = \exp\left(-\frac{\pi^2}{4}\left(t+2e^{-t}-\frac{1}{2}e^{-2t}-\frac{3}{2}\right)\right). \tag{4.3}$$

We refer the readers to [16] for more properties of this example.

First, we fix the number of moments to be 40. In Figs. 1, 2 and 3, the density ρ, macroscopic velocity u, the local temperature θ and heat flux q at $t=1$, 2 and 5 are plotted. The number of spatial grids we used are $N=160$, 320, 640, 1280, 2560. It is clear that with the increasing of the grid number, ρ, u, θ and q are converging to the analytic solution. In Fig. 4, the L^2 errors of ρ, u, θ and q at $t=1$, 2 and 5 between the numerical solution and the analytic solution are plotted, respectively. All errors are about linearly converging to zero with the increasing of the spatial grid number. In Fig. 5, the point-wise error

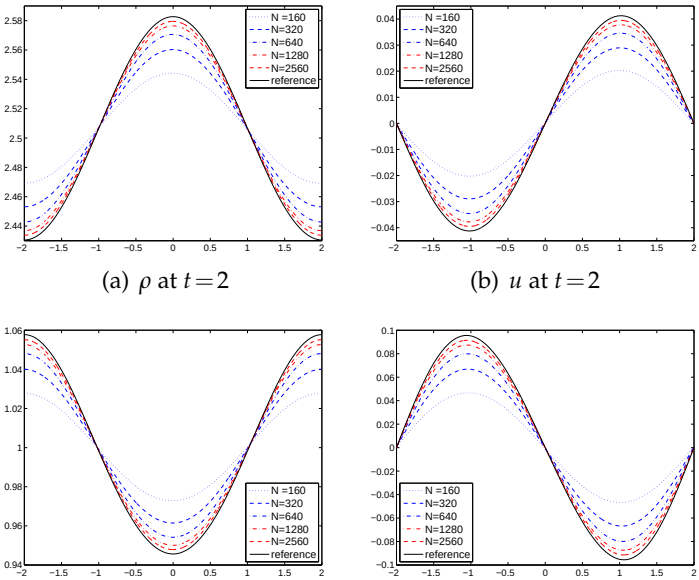
https://doi.org/10.4208/cicp.220415.080816a Published online by Cambridge University Press



(a) ρ at $t=1$ (b) u at $t=1$

(c) θ at $t=1$ (d) q at $t=1$

Figure 1: The density ρ, macroscopic velocity u, the temperature θ and the heatflux q of the particles of Eq. (4.1) on different spatial grids at $t=1$. The reference solution in the black line is the analytic solution of Eq. (4.1).

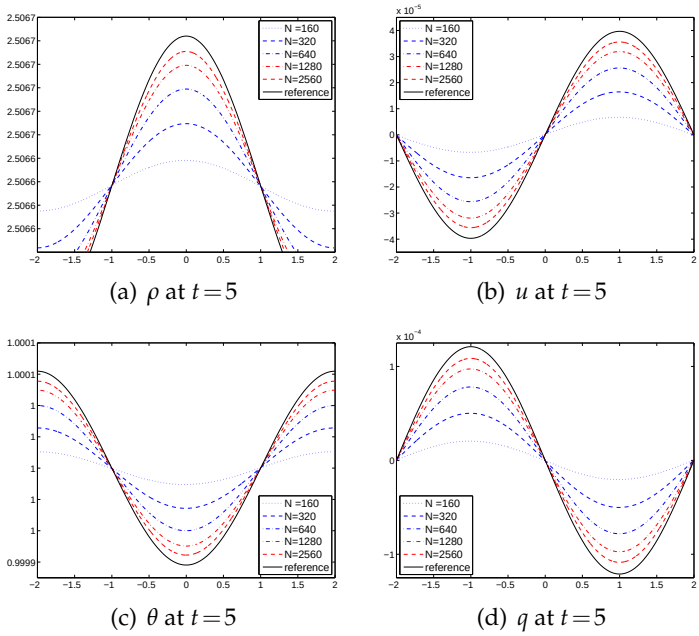


(a) ρ at $t=2$ (b) u at $t=2$

(c) θ at $t=2$ (d) q at $t=2$

Figure 2: The density ρ, macroscopic velocity u, the temperature θ and the heatflux q of the particles of Eq. (4.1) on different spatial grids at $t=2$. The reference solution in the black line is the analytic solution of Eq. (4.1).

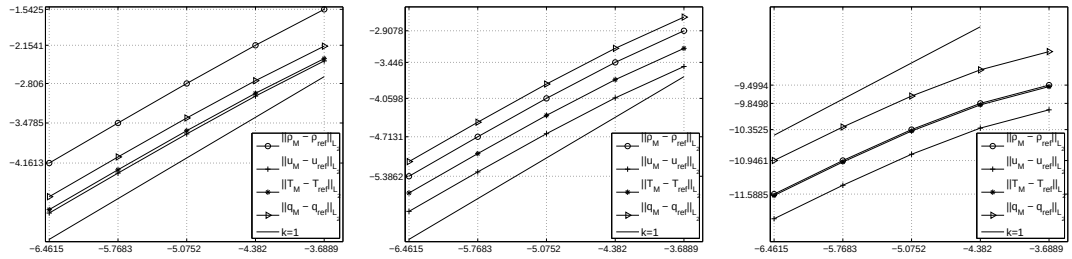
https://doi.org/10.4208/cicp.220415.080816a Published online by Cambridge University Press



(a) ρ at $t=5$ (b) u at $t=5$

(c) θ at $t=5$ (d) q at $t=5$

Figure 3: The density ρ, macroscopic velocity u, the temperature θ and the heatflux q of the particles of Eq. (4.1) on different spatial grids at $t=5$. The reference solution in the black line is the analytic solution of Eq. (4.1).

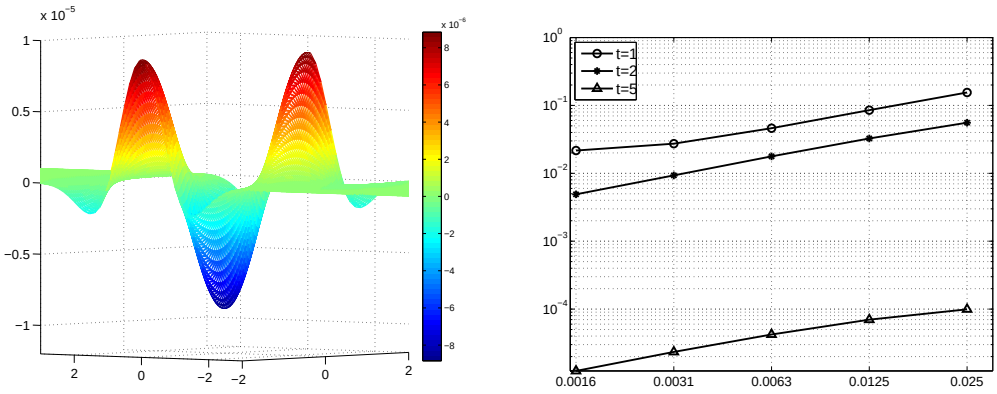


(a) $t=1$ (b) $t=2$ (c) $t=5$

Figure 4: The L^2 error of the density ρ, macroscopic velocity u, the local temperature θ and the heatflux q between the moment method using different spatial grid sizes and the analytic solution of Eq. (4.1) at $t=1$,2 and 5. The x-axis is $log(\Delta x)$, where Δx is the spatial grid size and the y-axis is $log(\mathcal{E}_{L^2})$, where $\mathcal{E}_{L^2}$ is the L^2 error between the numerical solution and the analytic solution.

of the distribution function between the numerical solution and the analytic solution at $t=5$ with grid number $N=2560$ and moment number $M=40$ is plotted. From it, we can see that the absolute point-wise error between the moment method and analytic solution is quite small. Further more, the L^2 errors of the distribution function between the numerical solution and the analytic solution at $t=1$, 2 and 5 are also plotted in Fig. 5. We can find that the numerical solutions obtained using the NRxx method are linearly converging to the analytic solution with the grid size going to zero.

https://doi.org/10.4208/cicp.220415.080816a Published online by Cambridge University Press



(a) $dis^h_M - dis_{ref}$ at $t=5$ (b) $\|dis^h_M - dis_{ref}\|_{L2}$

Figure 5: The error of the distribution function between the moment method and the analytic solution of Eq. (4.1). The left one is $(dis^h_M - dis^h_{ref})$ at $t=5$ with $N=2560$ and $M=40$. The right one is $\|dis^h_M - dis_{ref}\|_{L2}$ using different spatial grid size at $t=1$,2 and 5. In the left pic, the x-axis and the y-axis are the spatial space and the microscopic space respectively, and the z-axis is the error $(dis^h_M - dis^h_{ref})$. In the right pic, the x-axis is $log(\Delta x)$, where Δx is the spatial grid size and the y-axis is $log(\mathcal{E}_{L^2})$, where $\mathcal{E}_{L^2}$ is the L^2 error between the numerical solution and the analytic solution.

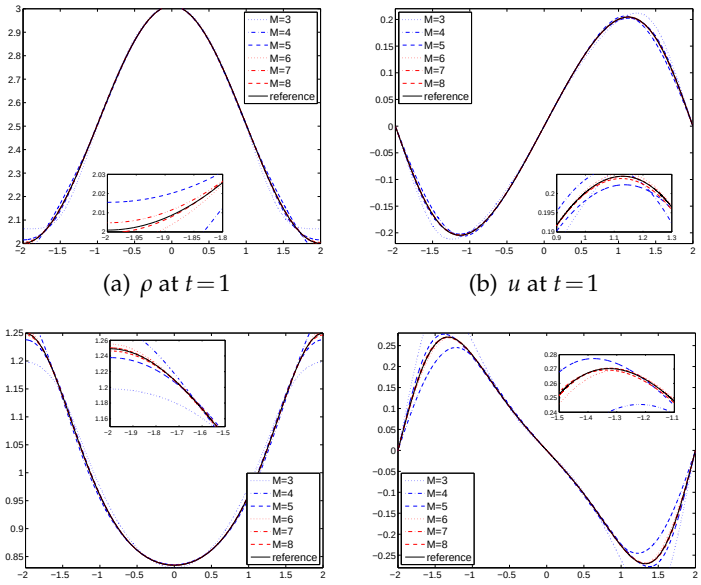
Then, let us turn to the study of the numerical convergence in terms of the number of moments. Again Eq. (4.1) is numerically solved. The results using different number of moment ranging from 3 to 8 are collected in Fig. 6 with the fixed number of spatial grids $N=10240$. We find that the numerical solutions are converging to the analytic solutions with the number of moments increasing. The exponential convergence rate with the number of moments is expected since the Hermite spectral expansion is used in the velocity space.

In Fig. 7, the L^2 errors of the distribution function between the numerical solutions and the analytic solutions with different moment number at $t=1$, 2, 5 with fixed number of spatial grids $N=20480$, which is the largest number we can afford, are plotted. From it, we can find that when the moment number is small, the numerical solutions are exponentially converging to the analytical solution. However, with the moment number increasing, the spatial error is the dominate error and we can no longer see the spectral convergence. Moreover, we have checked the variation of the coefficient in front of v in (4.2) with time increasing. From Fig. 8, we can find that the coefficient has reached the maximum at around $t=1$, and then is approximating to zero. And the distribution function is approximating to the equilibrium distribution with time increasing. This may be the reason why the convergence results are less satisfactory when $t=1$.

4.2 A Riemann problem

In this section, we apply our method to a Riemann problem with periodic boundary condition in the spatial space. The initial example is from [22, 33].

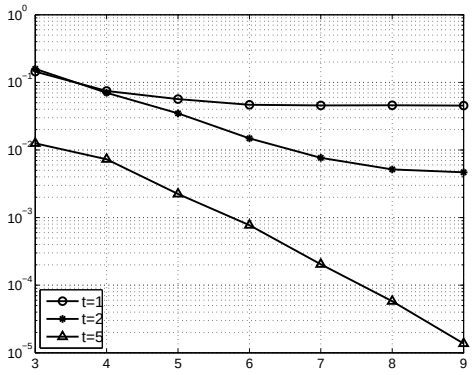
https://doi.org/10.4208/cicp.220415.080816a Published online by Cambridge University Press



(a) ρ at $t=1$ (b) u at $t=1$

(c) θ at $t=1$ (d) q at $t=1$

Figure 6: The density ρ, macroscopic velocity u, the temperature θ and the heatflux q of the particles of Eq. (4.1) with different number of moments at $t=1$. The reference solution in the black line is the analytic solution of Eq. (4.1). The number of grid is $N=10240$ and the number of moment is ranged from 3 to 8.

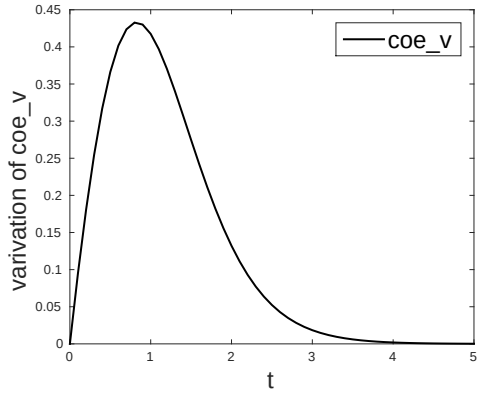


(a) $log(\|dis_M^h - dis_{ref}^h\|_{L^2})$

Figure 7: The moment error between the numerical solution using different number of moments and the analytic solution of the distribution function at $t=1,2,5$. The number of moment is varied from $M=3$ to $M=10$. The x-axis is the number of moments M and the y-axis is $log(\|dis_M^h - dis_{ref}^h\|_{L^2})$.

First, we will introduce the high-field model of the VPFP system. If the mean free path $l_e=\sqrt{\mu_e}\tau_e$ of the particles is much smaller than the Debye length $\Lambda=\sqrt{(\epsilon_0 k_B T_{th})/(q^2\mathcal{N})}$, where $\mathcal{N}$ is the typical value for the concentration of the particles, then system Eq. (2.1)

https://doi.org/10.4208/cicp.220415.080816a Published online by Cambridge University Press



(a) the variation of the coefficient of v

Figure 8: The variation of the coefficient in front of v in (4.2) with time increasing.

changes into

$$\partial_t f + \boldsymbol{v}\cdot\nabla_{\boldsymbol{x}} f - \frac{1}{\epsilon}\nabla_{\boldsymbol{x}}\phi\cdot\nabla_{\boldsymbol{v}} f = \frac{1}{\epsilon}\mathcal{L}_{FP}(f), \tag{4.4}$$

$$-\Delta_{\boldsymbol{x}}\phi = \rho - h, \tag{4.5}$$

where $\epsilon = \left(\frac{l_e}{\Lambda}\right)^2$ is the ratio between the mean free path l_e and the Debye length Λ, and the Fokker-Planck operator form $\mathcal{L}_{\mathcal{FP}}$ is deduced as:

$$\mathcal{L}_{\mathcal{FP}} = \nabla_{\boldsymbol{v}}\cdot(\boldsymbol{v}f + \nabla_{\boldsymbol{v}} f). \tag{4.6}$$

Under this scaling, let $\epsilon\to 0$, thus the so-call high-field limit of the VPFP system is derived. Then we can define the local Maxwellian as:

$$f_{\text{eq}} = \frac{\rho(t,\boldsymbol{x})}{(2\pi)^{N/2}}\exp\left(\frac{-|\boldsymbol{v}-\boldsymbol{u}(t,\boldsymbol{x})|^2}{2}\right), \tag{4.7}$$

where $\boldsymbol{u}(t,\boldsymbol{x})$ is the macroscopic velocity of the particles, and satisfies

$$\rho(t,\boldsymbol{x})\boldsymbol{u}(t,\boldsymbol{x}) = \int_{\mathbb{R}^N}\boldsymbol{v}f(t,\boldsymbol{x},\boldsymbol{v})\,\mathrm{d}\boldsymbol{v}. \tag{4.8}$$

Remark 4.1. When pushing ϵ in Eq. (4.4) to 0, the distribution f formally goes to Eq. (4.7) if we define

$$\boldsymbol{u}_{steady} = -\nabla_{\boldsymbol{x}}\phi. \tag{4.9}$$

Just as that in [22, 33], we are also interested in the 1D case of the high-field model:

$$\frac{\partial f}{\partial t} + v\frac{\partial f}{\partial x} - \frac{1}{\epsilon}\frac{\partial\phi}{\partial x}\frac{\partial f}{\partial v} = \frac{1}{\epsilon}\left(\frac{\partial(vf)}{\partial v} + \frac{\partial^2 f}{\partial v^2}\right), \tag{4.10}$$

$$-\frac{\partial^2\phi}{\partial x^2} = \rho - h. \tag{4.11}$$

https://doi.org/10.4208/cicp.220415.080816a Published online by Cambridge University Press

From the expansion Eq. (3.4) and the high-field model Eq. (4.4), the local Maxwellian Eq. (4.7) in the 1D case can be extended as

$$f_{\text{eq}} = f_0 \mathcal{H}_{\theta,0}\left(\frac{v-u}{\sqrt{\theta}}\right), \tag{4.12}$$

where

$$f_0 = \rho(t,x), \quad u = -\partial_x \phi, \quad \theta = 1, \tag{4.13}$$

is the density, macroscopic velocity and temperature of the particles respectively.

Here, the initial condition is as follows:

$$\begin{cases} (\rho_l, h_l) = (1/8, 1/2), & 0 \leqslant x < 1/4, \\ (\rho_m, h_m) = (1/2, 1/8), & 1/4 \leqslant x < 3/4, \\ (\rho_r, h_r) = (1/8, 1/2), & 3/4 \leqslant x \leqslant 1, \end{cases} \tag{4.14}$$

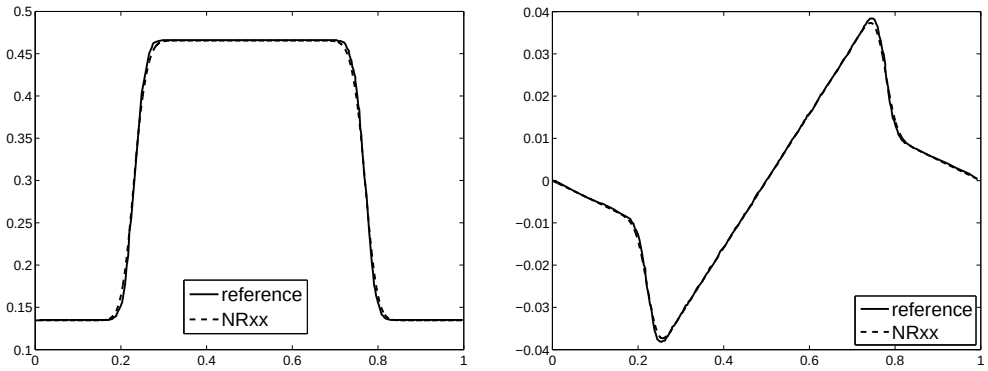
and the ϵ in Eq. (4.10) is fixed to be 10^{-3}. The initial distribution is

$$f(x,v,0) = \frac{\rho(x,0)}{\sqrt{2\pi}} \exp\left(-\frac{(v-u(x,0))^2}{2}\right), \tag{4.15}$$

where $u(x,0) = -\partial_x \phi$ and ϕ satisfies

$$-\partial_{xx}\phi = \rho(x,0) - h(x,0). \tag{4.16}$$

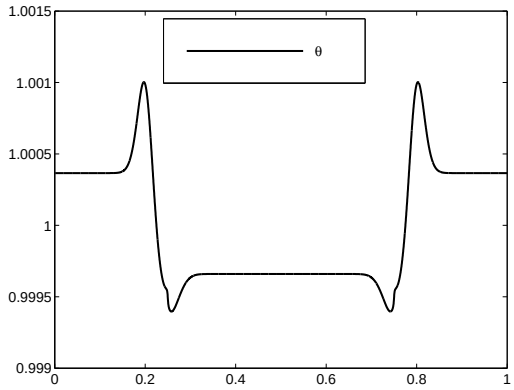
To validate the effect of the NRxx method, we compare the numerical results using the NRxx method with that in [20]. In Fig. 9, the density ρ, and the momentum ρu at $t = 0.2$ are plotted. Here, the grid size is $N = 500$ and the number of moment $M = 10$. The time step is almost $\Delta t = 2e(-4)$. From it, we can find that the numerical solutions match well with the reference solutions [22]. In Fig. 10, the temperature θ at $t = 0.2$ is plotted.



(a) ρ (b) ρu

Figure 9: The density ρ, and momentum ρu of the particles with the initial condition Eq. (4.14) at $t = 0.2$. The reference solution in the black line is the reference solution in [22].

https://doi.org/10.4208/cicp.220415.080816a Published online by Cambridge University Press



(a) θ

Figure 10: The temperature θ of the particles with the initial condition Eq. (4.14) at $t=0.2$.

4.3 Parameter study of the VPFP system

It is known that the solution to the VPFP system converges to a time independent steady solution as $t\to\infty$ [3]. In this section, we will demonstrate this property under the dimensionless form of the VPFP system Eq. (3.1) using the NRxx method. The effects of the two parameters β and γ are also discussed. The following initial distribution function from [31] is adopted

$$f_0(x,v)=\frac{K}{\sqrt{2\pi T_{th}}}\left(1+2\epsilon\cos\left(\frac{2\pi x}{L}\right)\right)\exp\left(\frac{-v^2}{2T_{th}}\right),\quad 0\leqslant x\leqslant L, \tag{4.17}$$

where T_{th},ϵ,L,K are constants and $h(x)=K$ in Eq. (3.1). It is known that if $\beta=\gamma=0$ in Eq. (3.1), the VPFP system reduces into VP equations, the solution of which represents classical Landau damping [11]. The physical mechanism of Landau damping is a transfer of energy from the wave to plasma particles that are moving with a velocity close to the phase velocity of the wave. However, if $\beta,\gamma\neq 0$, the solution of Eq. (3.1) approaches a steady state as below when $t\to\infty$:

$$f(x,v)=\frac{K}{\sqrt{2\pi\gamma}}\exp\left(\frac{-v^2}{2\gamma}\right). \tag{4.18}$$

This is for the reason that the diffusion in velocity space become dominant as time increases and finally the solution reaches the steady state. The electric energy and the kinetic energy are tested to observe the approach to the steady state. The electric energy is defined as:

$$\mathcal{E}(t)=\frac{1}{2}\int_0^L(\partial_x\phi)^2\mathrm{d}x. \tag{4.19}$$

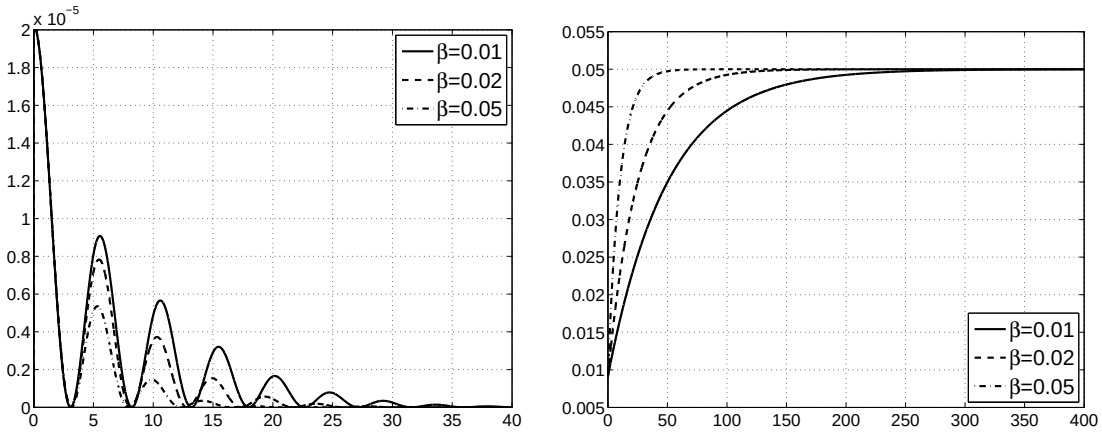
https://doi.org/10.4208/cicp.220415.080816a Published online by Cambridge University Press

At the steady state, $h(x)=K$ and $\rho-h(x)=0$, thus $\mathcal{E}(t)\to 0$, when $t\to\infty$. The kinetic energy is defined as

$$\mathcal{K}(t)=\frac{1}{2}\int_0^L\int_{-\infty}^{\infty}v^2f(t,x,v)\mathrm{d}v\mathrm{d}x=\frac{1}{2}(\rho u^2+\rho\theta). \tag{4.20}$$

From Eq. (4.18), we can derive that $2\mathcal{K}\to\gamma KL$, when $t\to\infty$.

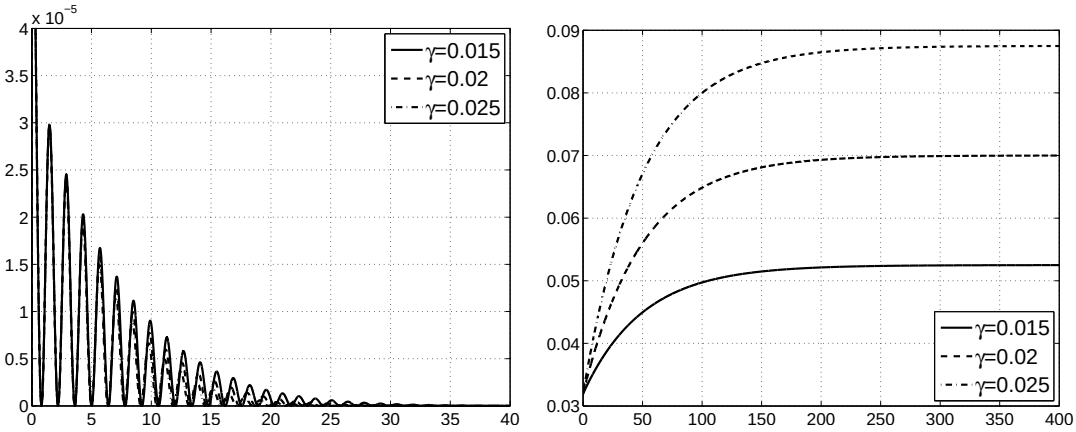
To demonstrate the time asymptotic behavior, we compute the solution to Eq. (3.1) with the initial function Eq. (4.17) for varying β and γ. First, we will consider the variance of β. Let $\epsilon=0.01$, $L=4$, $\sqrt{T_{th}}=0.3/\pi$, $K=1/4$, $\gamma=0.05$, and then take $\beta=0.01$,0.02 and 0.05. The variations of the $\mathcal{E}(t)$ and $\mathcal{K}(t)$ for different β are plotted in Fig. 11. For these computations, the grid size is $N=1600$ and the number of moment is $M=80$. From Fig. 11, we can find that the electric energies are all converging to zero with different velocities for different β and the problem with larger β is converging at a higher speed. The same conclusion can also be derived from the variations of $\mathcal{K}(t)$ for different β: the kinetic energy $\mathcal{K}(t)$ are converging to the steady state $2\mathcal{K}_{steady}=\gamma KL=0.05$. Secondly, we test the approach to the steady state with different γ. Let $\epsilon=0.01$, $L=1$, $K=3.5$, $\beta=0.01$ and $\gamma=0.015$, 0.02, 0.025. Then the steady states of the kinetic energy to those different γ is $\mathcal{K}_{steady}=0.525$, 0.07, 0.0875. The variations of $\mathcal{E}(t)$ and $\mathcal{K}(t)$ are plotted in Fig. 12. For these computations, the grid size is $N=1600$ and the number of moment is $M=40$. In Fig. 12, $\mathcal{E}(t)$ and $\mathcal{K}(t)$ are both converging to the steady state with different velocities and the problem with larger γ is converging at higher speed.



(a) $\mathcal{E}(t)$ (b) $\mathcal{K}(t)$

Figure 11: The variation of $\mathcal{E}$ and $\mathcal{K}$ with different β as $t\to\infty$. The parameters in Eq. (4.17) is $\epsilon=0.01$, $L=4$, $K=1/4$, $\sqrt{T_{th}}=0.3/\pi$, $\gamma=0.05$ and $\beta=0.01$, 0.025, 0.1. The x-axis is time T and the y-axis are $2\mathcal{E}$ and $2\mathcal{K}$ respectively.

https://doi.org/10.4208/cicp.220415.080816a Published online by Cambridge University Press



(a) $2\mathcal{E}(t)$ (b) $2\mathcal{K}(t)$

Figure 12: The variation of $\mathcal{E}$ and $\mathcal{K}$ with different γ as $t\to\infty$. The parameters in Eq. (4.17) is $\epsilon=0.01$, $L=1$, $K=3.5$, $\sqrt{T_{th}}=0.3/\pi$, $\beta=0.1$ and $\gamma=0.015$, 0.02, 0.025. The x-axis is time T and the y-axis are $2\mathcal{E}$ and $2\mathcal{K}$ respectively.

5 Conclusion

We extend the moment system derived from the Boltzmann transport equation to the VPFP system using the NRxx method, and then obtain a series of the high-order moment equations as an extension of the model in [11]. The conservation properties of the scheme are also discussed in this paper.

The numerical convergence with respect to the grid-size and the order of moments are studied. The linear convergence in grid-size and the exponential convergence in the number of moments are derived. A Riemann problem of the high-field model of the VPFP system is also tested. We have compared the numerical results obtained using NRxx method with that in [22]. The numerical results of our high-order moment methods agree well with that in [22]. Moreover, the approaches to the steady state with different parameters are observed using the NRxx method. The variations of the converging velocity with different β and γ are also obtained.

It is illustrated that the high-order moment system is a promising alternative to model the VPFP system. More complex form of the Fokker-Planck operator has to be considered to predict the movement of particles in plasma, and we are now investigating to the initial form of the Fokker-Planck operator by using the NRxx method.

Acknowledgments

We thank Prof. R. Li and Prof. T. Lu from Peking University for their helpful suggestions on this paper. This research of Y. Wang was supported in part by CAEP (Grant

https://doi.org/10.4208/cicp.220415.080816a Published online by Cambridge University Press

2013A0101004). And this research of S. Zhang was partly supported by NSFC 11472060 and NSFC 61431014.

References

[1] E.J. Allen and H.D. Victory Jr. A computational investigation of the random particle method for numerical solution of the kinetic Vlasov-Poisson-Fokker -Planck equations. *Physica A*, 209(3):318–346, 1994.
[2] F. Bouchut. Existence and uniqueness of a global smooth solution for the Vlasov-Poisson-Fokker-Planck system in three dimensions. *J. Funct. Anal*, 111:239–258, 1993.
[3] F. Bouchut. Smoothing effect for the non-linear Vlasov-Poisson-Fokker-Planck system. *J. Differ. Eq*, 122:225–238, 1995.
[4] Z. Cai, Y. Fan, and R. Li. Globally hyperbolic regularization of Grad's moment system in one dimensional space. *Comm. Math Sci.*, 11(2):547–571, 2013.
[5] Z. Cai, Y. Fan, and R. Li. Globally hyperbolic regularization of Grad's moment system. *Comm. Pure Appl. Math.*, 67(3):464–518, 2014.
[6] Z. Cai, Y. Fan, R. Li, T. Lu, and Y. Wang. Quantum hydrodynamics models by moment closure of wigner equation. *J. Math. Phys.*, 53:103503, 2012.
[7] Z. Cai and R. Li. Numerical regularized moment method of arbitrary order for Boltzmann-BGK equation. *SIAM J. Sci. Comput.*, 32(5):2875–2907, 2010.
[8] Z. Cai, R. Li, and Z. Qiao. Globally hyperbolic regularized moment method with applications to microflow simulation. *Comput. Fluids*, 81:95–109, 2013.
[9] Z. Cai, R. Li, and Y. Wang. An efficient NRxx method for Boltzmann-BGK equation. *J. Sci. Comput.*, 50(1):103–119, 2012.
[10] Z. Cai, R. Li, and Y. Wang. Numerical regularized moment method for high Mach number flow. *Commun. Comput. Phys.*, 11(5):1415–1438, 2012.
[11] Z. Cai, R. Li, and Y. Wang. Solving Vlasov equations using NRxx method. *SIAM J. Sci. Comput.*, 35(6):A2807–A2831, 2013.
[12] C. Cercignani, I.M. Gamba, J.W. JeromeW, and C.-W. Shu. Device benchmark comparisons via kinetic, hydrodynamic, and high-hield models. *Comput. Method. Appl. M*, 181(4):381–392, 2000.
[13] C. Z. Cheng and G. Knorr. The integration of the Vlasov equation in configuration space. *J. Comput. Phys*, 22:330–351, 1976.
[14] P. Degond. Global existence of smooth solutions of Vlasov-Fokker-Planck equation in 1 and 2 space dimensions. *Ann. Scient. Éc. Norm. Sup. 4^c Série*, 19:519–542, 1986.
[15] F. Filbet and L. Pareschi. Nummerical solution of the Fokker-Planck-Landau equation by spectral methods. *Comm. Math. Sciences*, 1(1):208–209, 2003.
[16] J. Fok, B. Guo, and T. Tang. Combined Hermite spectral-finite difference method for the Fokker-Planck equation. *Math. Comput*, 71(240):1497–1528, 2002.
[17] T. Goudon, J. Nieto, F. Poupaud, and J. Soler. Multidimensional high-field limit of the electrosatic Vlasov-Poisson-Fokker-Planck system. *J. Diff. Eq.*, 213:418–442, 2005.
[18] K.J. Havlak and H.D. Victory Jr. The numerical analysis of random particle methods applied to Vlasov-Poisson Fokker-Planck kinetic equations. *SIAM J. Number. Anal*, 1:291–317, 1996.
[19] K.J. Havlak and H.D. Victory Jr. On deterministic particle methods for solving Vlasov–Poisson–Fokker–Planck systems. *SIAM J. Number. Anal*, 35(4):1473–1519, 1998.
[20] J. Hu, S. Jin, and B. Yan. A numerical scheme for the quantum Fokker-Planck-Landau equation efficient in the fluid regime. *Commn. Comp. Phys.*, 12:1541–1561, 2012.

https://doi.org/10.4208/cicp.220415.080816a Published online by Cambridge University Press

[21] Z. Hu, R. Li, T. Lu, Y. Wang, and W. Yao. Simulation of an n^+-n-n^+ diode by using globally-hyperbolically-closed high-order moment models. *J. Sci. Comput*, 59(3):761–774, 2014.
[22] S. Jin and L. Wang. An asymptotic preserving scheme for the Vlasov-Poisson-Fokker-Planck system in the high field regime. *Acta. Math. Sci*, 31(6):2219–2232, 2011.
[23] R. Li, T. Lu, Y. Wang, and W. Yao. Numerical method for high order hyperbolic moment system of Wigner equation. *Commun. Comput. Phys*, 15(3):569–595, 2013.
[24] H. Neunzert, M. Pulvirenti, and L. Triolo. On the Vlasov-Fokker-Planck equation. *Math. Meth. Appl. Sci.*, 6:527538, 1984.
[25] F. Poupaud and J. Soler. Parabolic limit and stability of the Vlasov–Fokker–Planck system. *Math. Mol. Meth. Appl. S*, 10:1027–1045, 2000.
[26] R. Rautmann. On the uniqueness and stability of weak solutions of a Fokker-Planck-Vlasov equation. In *Numerical Treatment of Differential Equations in Applications*, pages 141–150. Springer, 1978.
[27] J. Schaeffer. A difference scheme for the Vlasov-Poisson-Fokker-Planck system. *Research Report No. 97-NA-004, Department of Mathematical Sciences, Carnegie Mellon University*, 1997.
[28] J. Schaeffer. Convergence of a difference scheme for the Vlasov–Poisson–Fokker–Planck system in one dimension. *SIAM J. Number. Anal*, 35(3):1149–1175, 1998.
[29] J. W. Schumer and J. P. Holloway. Vlasov simulation using velocity-scaled Hermite representations. *J. Comput. Phys.*, 144(2):626–661, 1998.
[30] L. Triolo. Global existence for the Vlasov-Poisson/Fokker-Planck equation in many dimensions, for small data. *Math. Method. Appl. Sci*, 10(4):487–497, 1988.
[31] S. Wollman and E. Ozizmir. Numerical approximation of the Vlasov–Poisson–Fokker–Planck system in one dimension. *J. Comput. Phys*, 202:602–644, 2005.
[32] S. Wollman and E. Ozizmir. Numerical approximation of the Vlasov–Poisson–Fokker–Planck system in two dimensions. *J. Comput. Phys*, 228:6629–6669, 2009.
[33] B. Yan and S. Jin. A successive penaltybased asymptotic-preserving scheme for kinetic equations. *SIAM J. Sci. Comput.*, 35:A150–A172, 2013.
[34] G. Dal Maso, P. G. LeFloch, and F. Murat. Definition and weak stability of nonconservative products. *J. Math. Pures Appl.*, 74(6):483–548, 1995.
[35] S. Rhebergen, O. Bokhove, and J. J. W. van der Vegt. Discontinuous Galerkin finite element methods for hyperbolic nonconservative partial differential equations. *J. Comput. Phys.*, 227(3):1887–1922, 2008.
[36] Z. Cai, R. Li, and Z. Qiao. NRxx simulation of microflows with Shakhov model. *SIAM J. Sci. Comput.*, 34(1):A339–A369, 2012.
[37] S. Wollman and E. Ozizmir. A deterministic particle method for the Vlasov–Poisson–Fokker–Planck equation in one dimension. *J. Comput. Phys*, 213:316–365, 2008.

https://doi.org/10.4208/cicp.220415.080816a Published online by Cambridge University Press